# Sheffield Hallam University

# Complimentary Metal-Oxide-Semiconductor compatible deposition of nanoscale transition-metal nitride thin films for plasmonic applications

BOWER, Ryan, LOCH, Daniel <http://orcid.org/0000-0003-3252-0142>, WARE, Ecaterina, BERENOV, Andrey, ZOU, Bin, HOVSEPIAN, Papken, EHIASARIAN, Arutiun and PETROV, Peter

This document is the Supplemental Material

# Supporting Information

# Contents

# 1) Deposition parameters and analysis

Films were deposited using the following deposition parameters:

| Film | Number of Operating Cathodes | Peak Current (A) | |
|---|---|---|---|
| | | Ti target | Nb target |
| TiN | 1 | 45 | - |
| TiNbN co-sputter | 2 simultaneously | 45 | 35 |
| TiN/NbN 10nm layers | 1 at a time | 45 | 35 |
| TiN/NbN 20nm layers | 1 at a time | 45 | 35 |
| NbN | 1 | - | 35 |

Table 1: HIPIMS deposition parameter summary.

The sputtering target diameter was 100 mm, Ti purity was 99.6% and Nb purity was 99.9%. The target to substrate distance is 90 mm. The substrate temperature was measured using a thermocouple positioned 5 mm behind the substrate holder and calibrated for the surface of a Si substrate. The base pressure was $3\times10^{-6}$ Pa. Nitrogen and argon gas purity was 99.998% (N2.7). For all runs, the total pressure during deposition was maintained at 0.3 Pa by a PID controlled pump throttle valve. The Ar and $N_2$ gas flow ratio $qV(Ar):qV(N_2)$ was kept at 30:1 for single and multilayer depositions. For co-sputtering runs, the gas flow ratio was adjusted to 15:1 to compensate for higher reactive gas consumption of the two cathodes operating simultaneously. The substrates were at floating potential (no bias potential was applied to them). Substrates were chemically cleaned by standard acetone, IPA and deionised water wash in an ultrasonic bath before loading into the cluster system. The next step prior to deposition, was to plasma clean substrates by inverse sputter etching with argon to ensure all surface contaminants are removed and finally transported *in vacuo* to the deposition chamber.
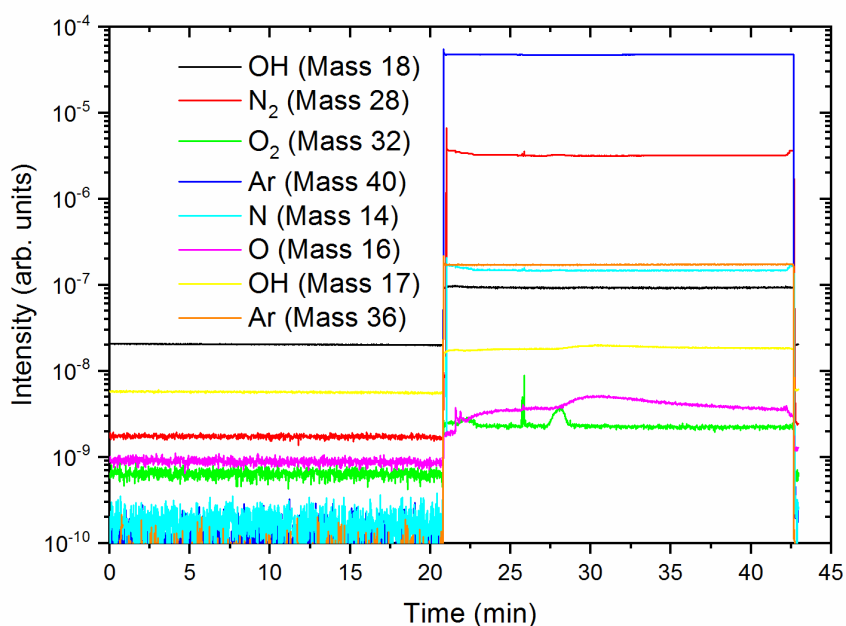


*Figure S1.1 : Residual Gas Analysis data for TiN deposition*

Residual Gas Analysis (RGA) data collected during each deposition indicates that the $O_2$ and OH partial pressures within each run were kept below $3\times10^{-5}$ Pa and $7.5\times10^{-4}$ Pa respectively. The data for the TiN deposition process is shown in Figure S1.1. Process gases Ar and $N_2$ are admitted at 21 minutes resulting in increased content of oxygen and water vapour in the chamber. When plasma power is turned off at the end of the process there is a slight increase in $N_2$ content due to the end of the reaction with the metal target. This is followed shortly by a switch off of the gas flow and the stop of data collection.
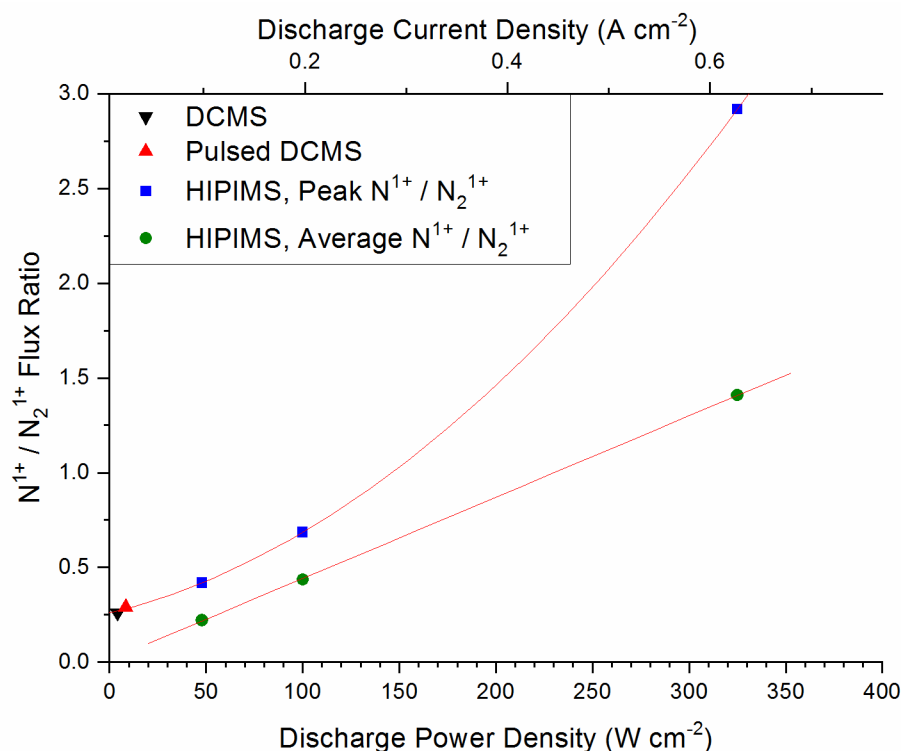


*Figure S1.2: Plasma sampling mass spectroscopy of TiN deposition. Squares indicate the ratio obtained at the peak of the HIPIMS pulse. Circles indicate the ratio obtained as a time-averaged measurement through the duration. Triangles indicate values for DC magnetron sputtering and pulsed DC magnetron sputtering.*

Plasma sampling mass spectroscopy of TiN deposition processes showed that the discharge power density resulted in an exponential increase in the $N^{1+}$ / $N_2^{1+}$ ion flux ratio observed during the peak of the pulse (Figure S1.2). The same ratio collected as an average throughout the pulse increased linearly with power density. At powers below 200 Wcm$^{-2}$, corresponding to low HIPIMS powers as well as DC magnetron sputtering (~10 Wcm$^{-2}$) and pulsed DC magnetron sputtering (~20 Wcm$^{-2}$) , the dissociation rate of nitrogen is insufficient. At high HIPIMS power, the dissociation rate is enhanced by an order of magnitude compared to conventional DC magnetron sputtering due to a comparable increase in plasma density and a higher probability of dissociative collisions.

## 2) Stoichiometric analysis

### a) Energy dispersive X-ray spectroscopy

| Sample | Ti at.% | Nb at.% |
|---|---|---|
| TiNbN | 49.7 | 50.3 |
| TiN/NbN 10nm layers | 52.4 | 47.6 |
| TiN/NbN 5nm layers | 52.75 | 47.25 |

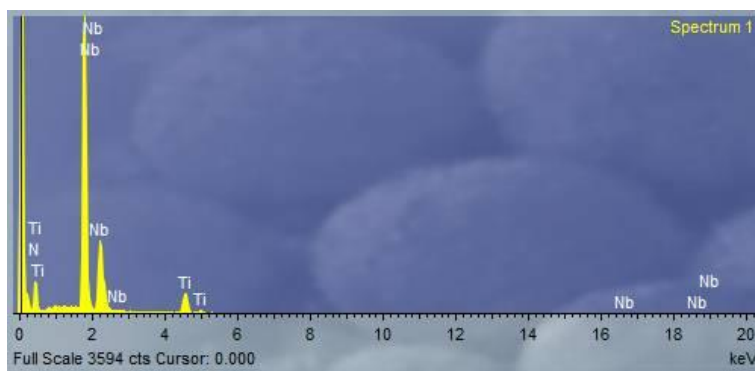*Table S2.1: EDX stoichiometries for Ti and Nb in layered and co-sputtered films*



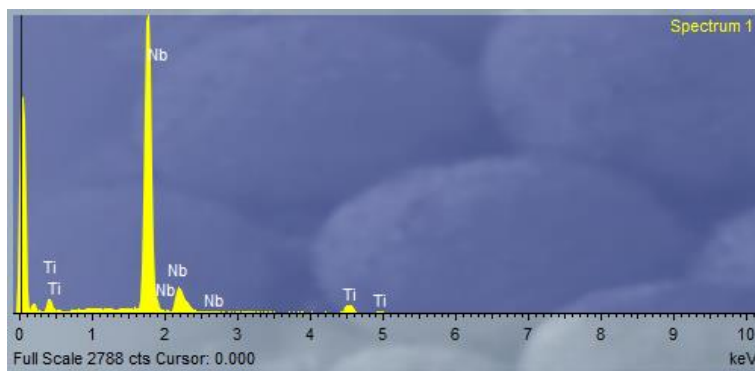*Figure S2.1: EDX spectrum for TiNbN on Si*



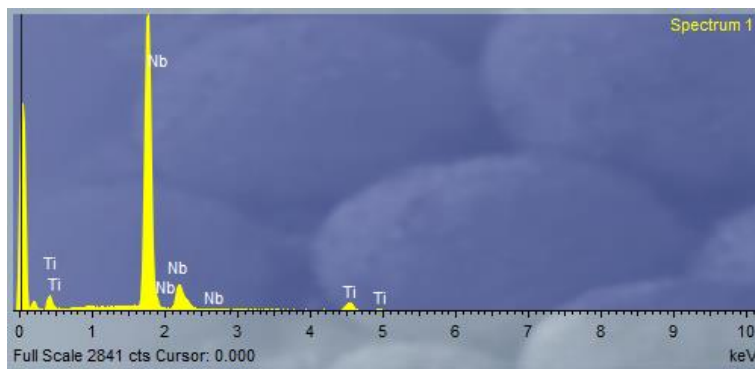*Figure S2.2: EDX spectrm for TiN/NbN on Si (10nm layers)*



*Figure S2.3: EDX spectrum for TiN/NbN on Si (5nm layers)*

b) XRF spectrum for co-sputtered thin films and binary thin films film

| Sample | Ti at. % | Nb at. % |
|--------|----------|----------|
| TiN | 99.1% | 0.1% |
| NbN | 2.9% | 97.1% |
| TiNbN | 48.1% | 51.9% |

*Table S2.2: XRF stoichiometries for Ti and Nb in binary and ternary films*
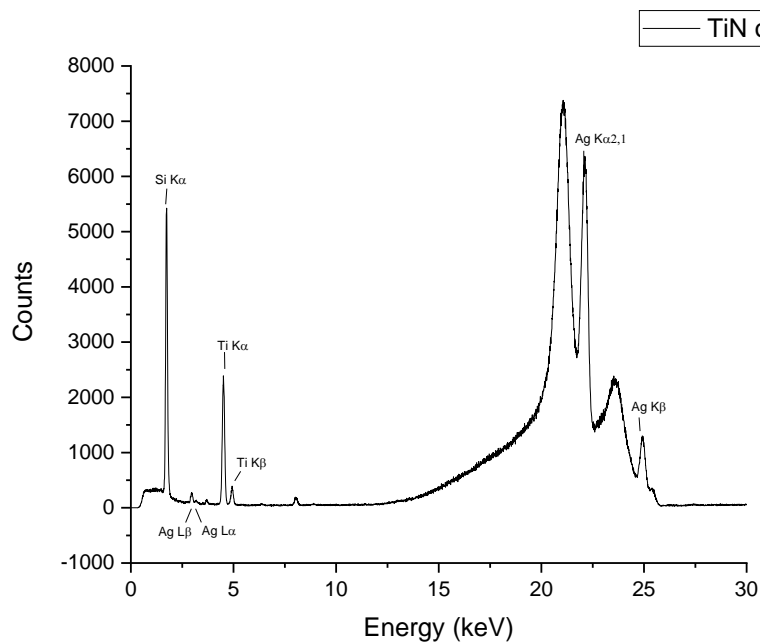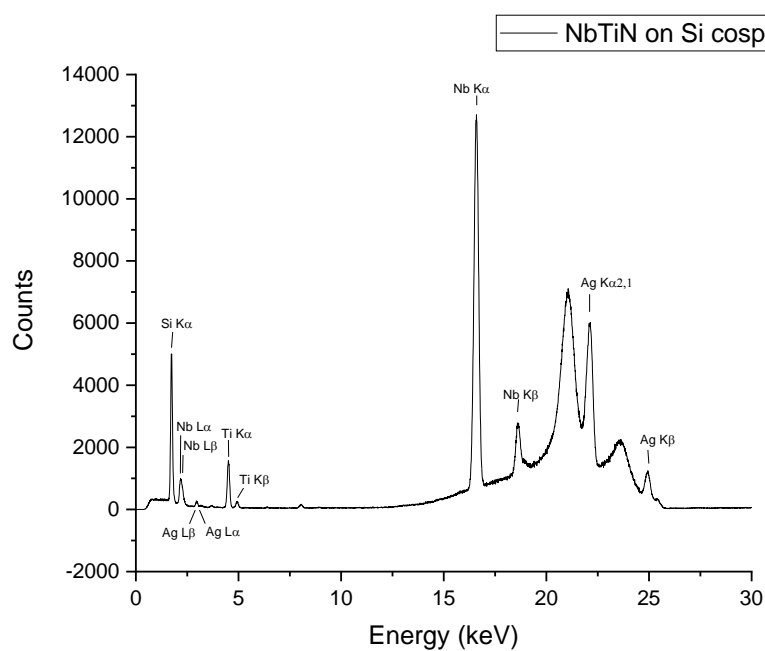


*Figure S2.4: XRF spectrum for TiN  on Si*



*Figure S2.5: XRF spectrum for TiNbN  on Si*
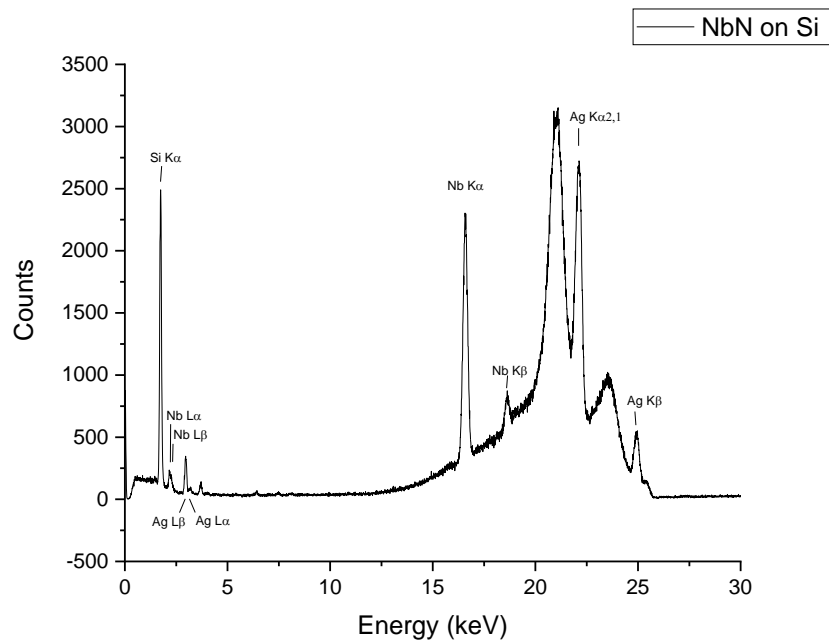
*Figure S2.6: XRF spectrum for NbN on Si*

The sharp Ag peaks visible in the XRF data are due to the primary AG source used. Additionally, the broad peaks observed at approximately 20 keV and 24 keV are a result of Compton scattering. The presence of Ti in the NbN and Nb in the TiN films is an artefact from the measurement software and is indicative of the accuracy of the technique.

# 3) Structural analysis (XRD)



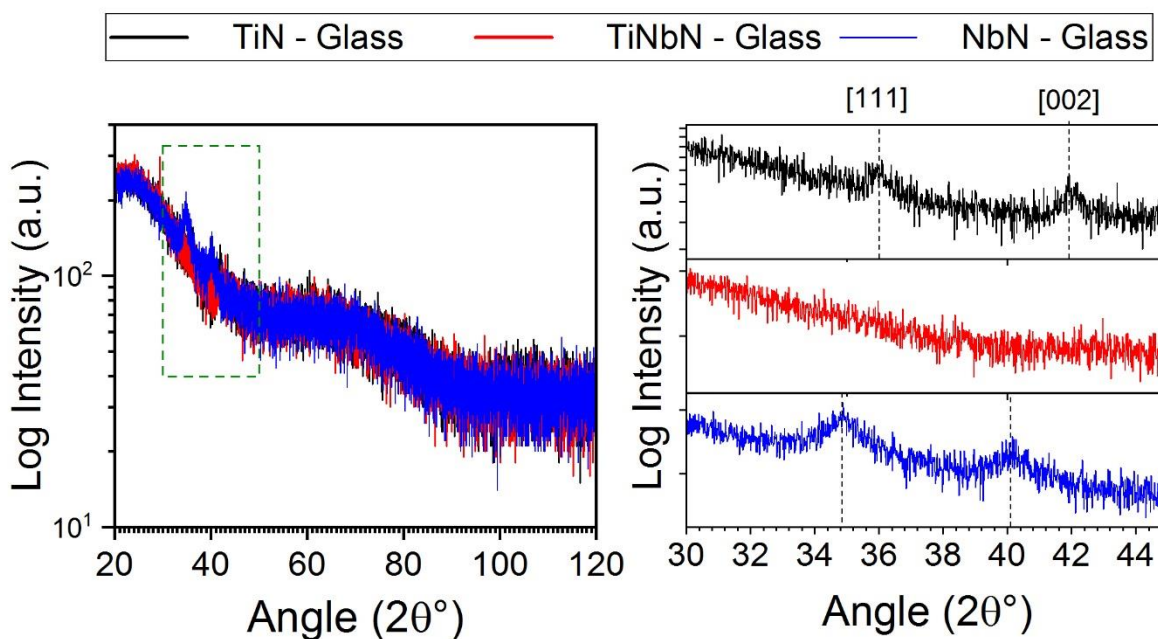*Figure S3.1: Thin film XRD of NbN. TiN and NbTiN films deposited on glass. Left shows full 2ϑ range, and right Inset displaying [111] and [002] peaks for the TMN films, demonstrating the change in lattice parameter with cation stoichiometry and identity. Dashed lines indicating peak position are included as a guide to the eye.*
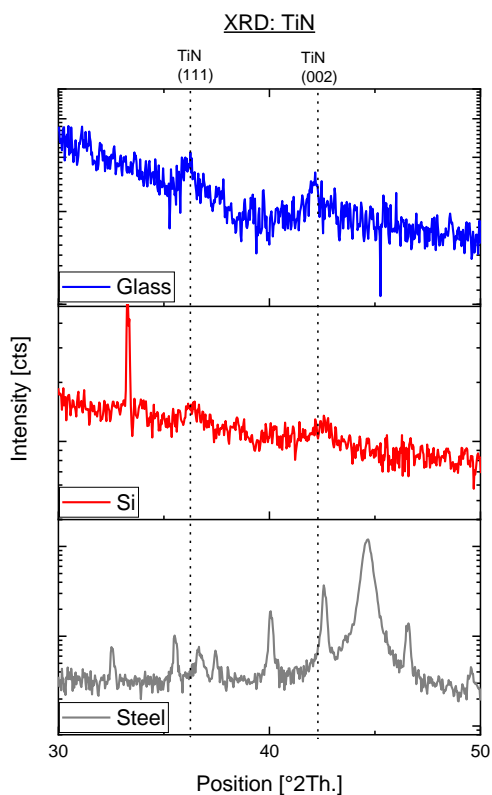


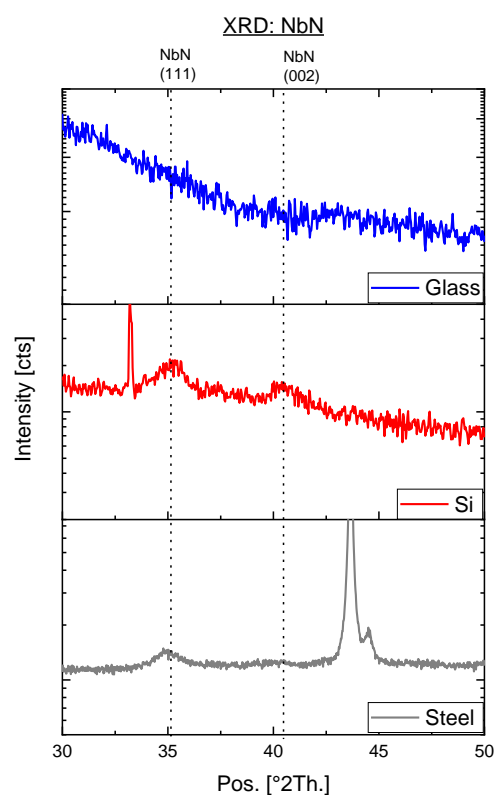Figure S3.2: XRD data for TiN films



Figure S3.3: XRD data for NbN films
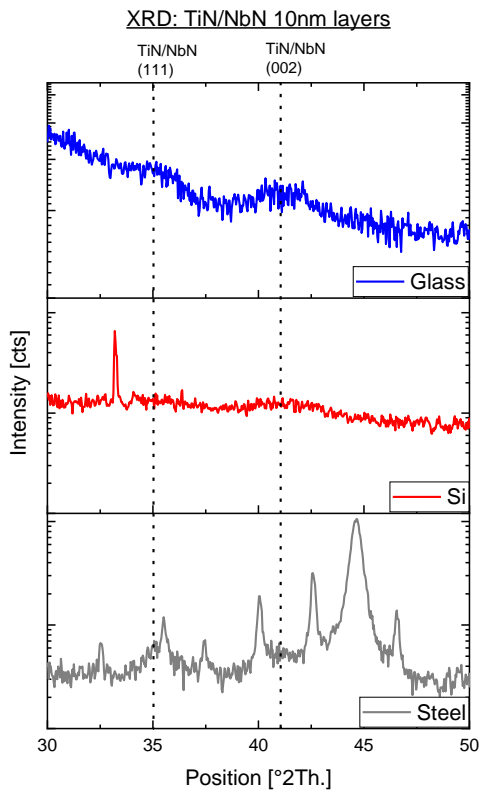
Figure S3.4: TiN/NbN layered films XRD data
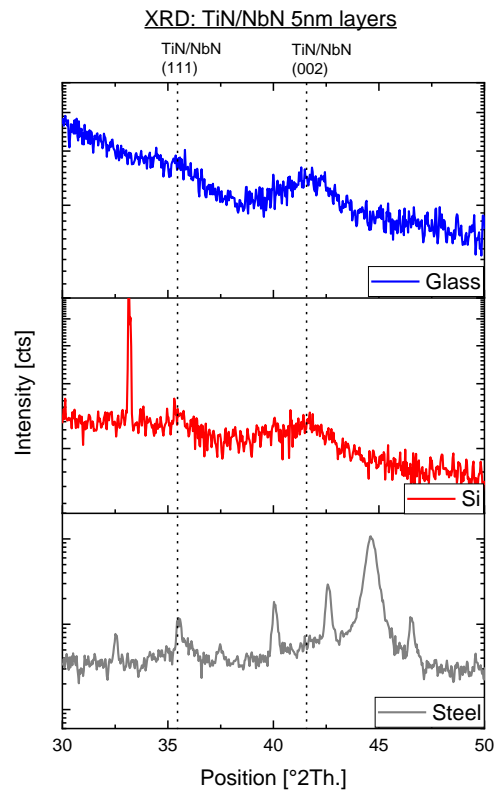


Figure S3.5: TiN/NbN layered films XRD data
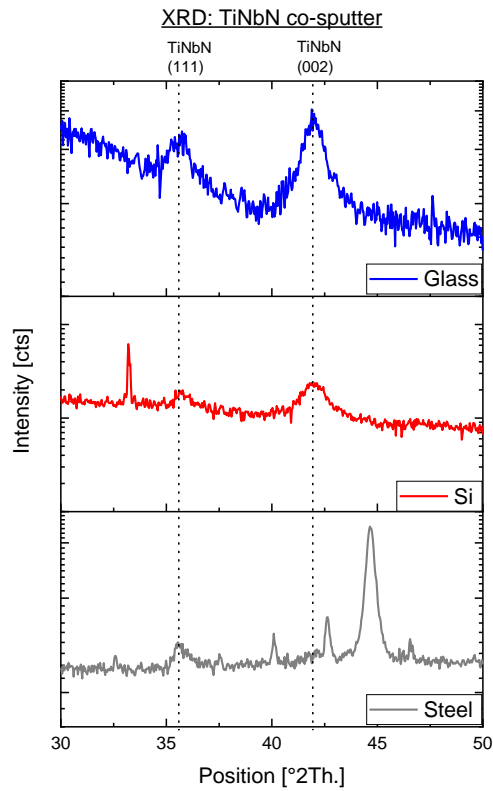


Figure S3.6: TiNNbN co-sputtered films XRD data

Table S3.1: Lattice parameters extracted from XRD data

All peaks in the XRD data not indexed as belonging to the thin films are from the substrate.

| Sample | Substrate | Lattice Parameter (Å) |
|---|---|---|
| NbN | Glass | - |
| | Si | 4.42 |
| | Steel | 4.46 |
| | MgO | 4.44 |
| TiN | Glass | 4.28 |
| | Si | 4.29 |
| | Steel | 4.25 |
| | MgO | 4.24 |
| TiNbN | Glass | 4.32 |
| | Si | 4.32 |
| | Steel | 4.33 |
| | MgO | 4.33 |
| TiN/NbN 5nm layers | Glass | 4.35 |
| | Si | 4.35 |
| | Steel | 4.39 |
| TiN/NbN 10nm layers | Glass | 4.39 |
| | Si | - |
| | Steel | 4.36 |

## 4) Surface Morphology: AFM
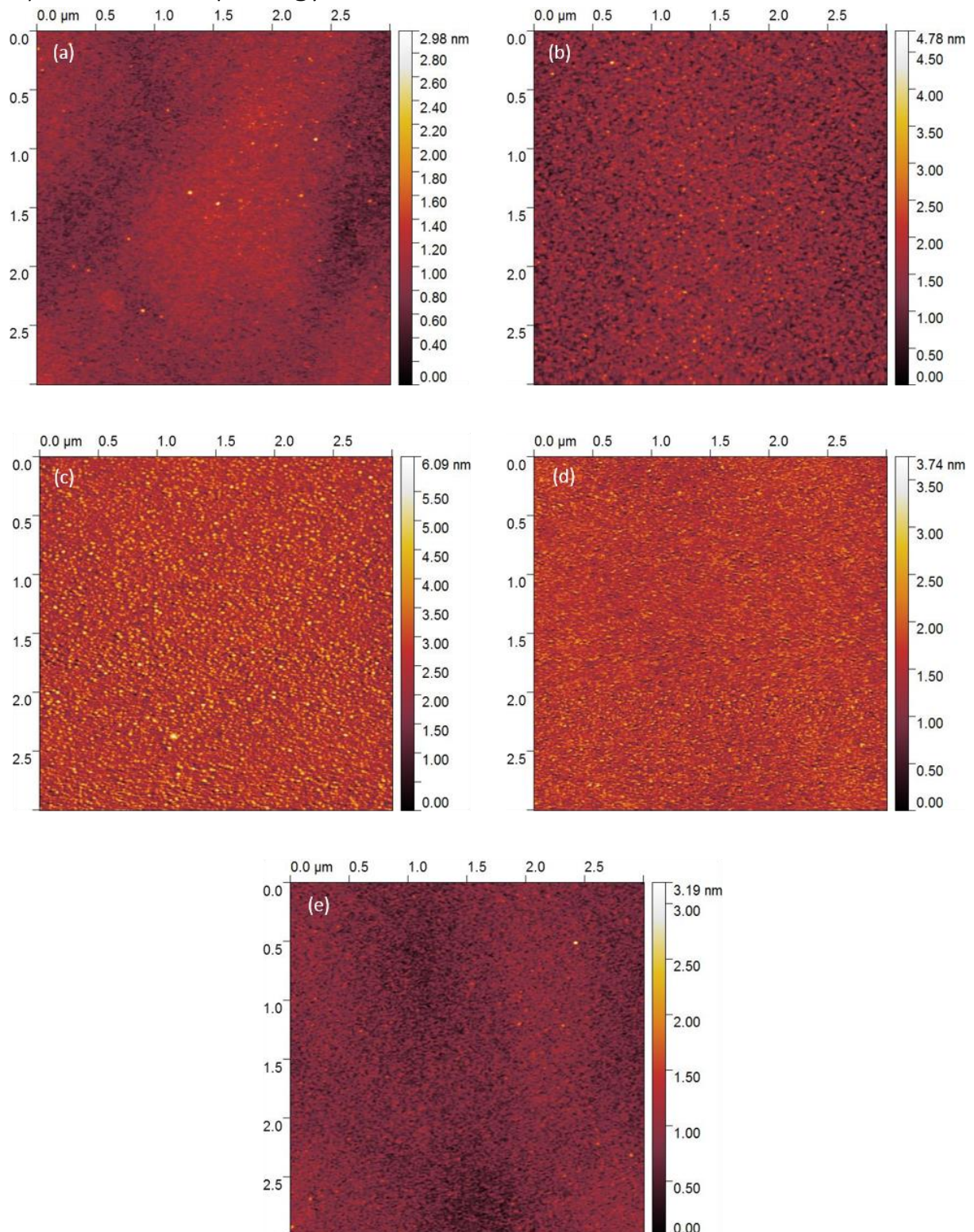


Figure S4: (a) NbN on Si. RMS = 0.189 nm; (b) TiNbN on Si. RMS = 0.35 nm; (c) TiN on Si. RMS = 0.666 nm; (d) TiN/NbN 10nm layers. RMS = 0.344 nm; (e) TiN/NbN 5nm layers. RMS = 0.195 nm

| Sample | RMS (nm) | Mean roughness (nm) |
|---|---|---|
| NbN | 0.189 | 0.150 |
| TiN/NbN layers (5nm) | 0.195 | 0.15 |
| TiN/NbN layers (10nm) | 0.344 | 0.270 |
| TiNbN | 0.35 | 0.28 |
| TiN | 0.666 | 0.52 |

Table S4.1: AFM surface roughness data for films on Si substrates

# 5) Ellipsometry Fitting

## a) Drude-Lorentz Fitting process

Ellipsometry data was fit using a Drude-Lorentz model of the form:

$$\varepsilon'(\omega) + i\varepsilon''(\omega) = \varepsilon_\infty - \frac{\omega_{pu}^2}{\omega^2 - i\Gamma_D} + \sum_{j=1}^{n} \frac{f_j \omega_{0_j}^2}{\omega_{0_j}^2 - \omega^2 + i\gamma_j \omega}$$

Where $\varepsilon_\infty$ relates to background absorption and $\omega_{pu}$ and $\Gamma_D$ are the unscreened plasma frequency and Drude broadening. The Lorentz oscillators are defined by the oscillator energy, strength, and damping: $\omega_j$, $f_j$, and $\gamma_j$ respectively.

A total of 2 Lorentz oscillators were used, as the inclusion of a third oscillator did not significantly improve the fit, as determined by the MSE.

It should be noted that for some films deposited on transparent substrates, the Lorentz oscillator term displays large widths ($\gamma_j$) which is likely indicative of inadequacies of the model fit. The model could likely be improved by considering contributions from a surface oxide layer. For layered films, accurate modelling of multiple reflections has not been included due to the complexity of the model required. Such analysis could further improve the fit to the experimental data.

| Sample | Substrate | MSE | $\varepsilon_\infty$ | $E_{pu}$ (eV) | $\Gamma_D$ (eV) | $E_1$ (eV) | $f_1$ | $\gamma_1$ (eV) | $E_2$ (eV) | $f_2$ | $\gamma_2$ (eV) |
|---|---|---|---|---|---|---|---|---|---|---|---|
| TiN | Steel | 8.123 | 2.856 | 6.71 | 0.408 | 6.199 | 9.3 | 95 | 4.647 | 2.803 | 1.915 |
| | Glass | 6.461 | 3.506 | 7.26 | 0.338 | 5.644 | 12.26 | 96 | 4.669 | 2.806 | 1.813 |
| | Si | 5.557 | 3.558 | 7.44 | 0.416 | 4.802 | 3.819 | 2.4 | 2.024 | 0.997 | 1.617 |
| | MgO | 5.986 | 3.295 | 7.17 | 0.325 | 4.442 | 14.157 | 64.3 | 4.776 | 3.033 | 1.945 |
| NbN | Steel | 1.014 | 2.454 | 13.43 | 3.849 | 5.911 | 2.684 | 2 | 0.57 | 3.022 | 0.603 |
| | Glass | 3.019 | 2.430 | 12.67 | 3.849 | 8.662 | 5.216 | 6.6 | - | - | - |
| | Si | 1.441 | 1 | 10.58 | 3.222 | 5.666 | 2.291 | 2.03 | 3.035 | 7.174 | 5.5 |
| | MgO | 1.494 | 1 | 12.45 | 3.591 | 6.791 | 4.151 | 2.66 | - | - | - |
| TiNbN | Steel | 2.73 | 1 | 8.49 | 0.986 | 6.9 | 0.15 | 6.082 | - | - | - |
| | Glass | 1.613 | 2.319 | 8.71 | 0.920 | 9.78 | 2.08 | 45.1 | 5.739 | 4.051 | 3.37 |
| | Si | 1.516 | 1.896 | 8.67 | 0.954 | 6.158 | 5.547 | 4.525 | 2.254 | 0.224 | 1.71 |
| | MgO | 1.993 | 2.763 | 8.57 | 0.863 | 9.596 | 2.203 | 46.77 | 5.371 | 3.619 | 2.922 |
| TiN/NbN 10nm layers | Steel | 6.599 | 2.326 | 8.5 | 0.852 | 3.535 | 0.284 | 10 | 5.123 | 0.259 | 1.64 |
| | Glass | 6.792 | 2.251 | 9.06 | 0.744 | 3.016 | 0.567 | 10 | 5.482 | 0.244 | 1.951 |
| | Si | 4.22 | 2.624 | 8.71 | 0.826 | 3.091 | 0.471 | 10 | 5.339 | 0.23 | 2.092 |
| | MgO | 2.93 | 2.176 | 9.01 | 0.766 | 2.24 | 1.179 | 6.7 | 5.977 | 0.213 | 2.88 |
| TiN/NbN 5nm layers | Steel | 2.36 | 1.154 | 8.82 | 0.709 | 1.509 | 2.66 | 3.15 | 6.795 | 0.144 | 5.718 |
| | Glass | 1.98 | 1.046 | 9.08 | 0.623 | 1.277 | 7.343 | 3.26 | 7.466 | 0.133 | 6.336 |
| | Si | 1.847 | 2.193 | 9.16 | 0.629 | 1.302 | 6.713 | 1.3 | 6.262 | 0.173 | 4.699 |
| | MgO | 3.834 | 2.513 | 8.99 | 0.812 | 3.276 | 0.34 | 10 | 5.458 | 0.239 | 2.025 |

Table S5.1: Ellipsometry fitting data for all films.
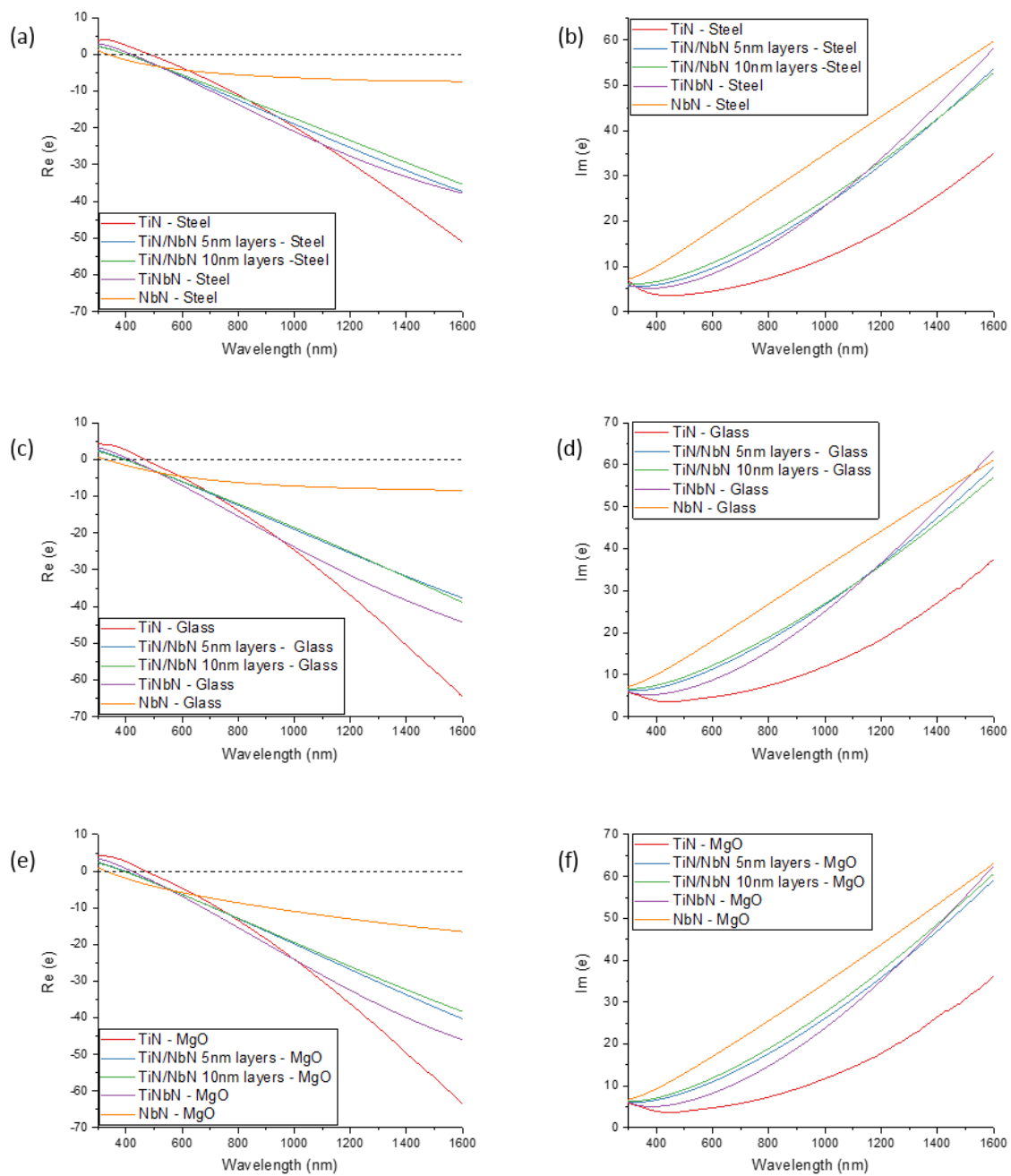
b) Ellipsometry data film comparison



Figure S5.1: Real and imaginary permittivity for steel (a, b), glass (c, d) and MgO (e, f) substrate films. Note that the steel substrates are conductive and the dielectric function observed may be affected by the substrate. This has not been considered in the ellipsometric fitting process used above.